ACS OMEGA

http://pubs.acs.org/journal/acsodf

Article

Morphologically Controlled Synthesis of Reduced-Dimensional ZnO/$Zn(OH)_2$ Nanosheets

Gyu Hyun Jeong, Hye Soung Jang, Jong Chan Yoon, Zonghoon Lee, Jieun Yang, A-Rang Jang,* and Gyeong Hee Ryu*

Cite This: *ACS Omega* 2022, 7, 35834−35839

Read Online

ACCESS | Metrics & More | Article Recommendations | Supporting Information

ABSTRACT: Conventional two-dimensional materials either have natural layered structures or are produced, with large surface areas, via physical or chemical synthesis. However, to form a two-dimensional material from a non-layered material, a method different from the existing ones is required. In this study, a surfactant-assisted method was utilized to synthesize $Zn(OH)_2$ (a nonlayered transition metal oxide) nanosheets. This study described the synthesis of $Zn(OH)_2$ nanosheets using an anionic sulfate layer and demonstrated a method of controlling the thickness and shape of the synthesized nanosheets by varying the surfactant concentration. Further, the characteristics of oxygen evolution reaction using ZnO/$Zn(OH)_2$ nanosheets, obtained by annealing the synthesized sheets, as catalysts were studied.

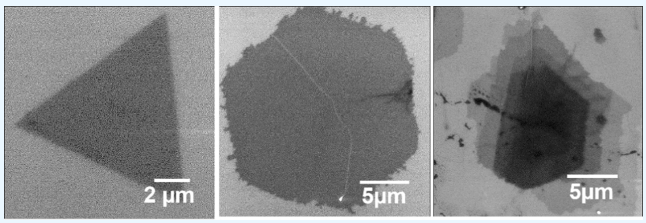

INTRODUCTION

Nanomaterials exhibit physical properties different from their bulk counterparts, especially when their thickness is reduced to atomic-scale layers. Conventional two-dimensional (2D) materials, such as graphene and transition metal dichalcogenides, are used in a variety of 2D nanostructures in electronic, optoelectronic, and electrochemical devices.[1−8] Following the successful isolation of graphene with unique properties, the study of 2D materials has gained particular importance in the fields of nanoscience and nanotechnology. Most of these actively utilized 2D materials have a naturally layered structure, and as such, are obtained by either physical or chemical synthesis over a large area.[9−11] However, to form 2D materials from non-layered materials, a method different from the existing ones is required. Previous research has proposed a surfactant-assisted method,[12−14] which allows non-layered materials with crystal structures, such as wurtzite and rock salt, to be synthesized into materials with nanoscale thinness.[15−18] Therefore, an effective synthesis method for the growth of large-area 2D nanosheets is practically feasible for several novel material applications.

Several nonlayered materials can be synthesized as 2D materials using the above-mentioned method. Among them, ZnO, which is a transition metal oxide, can be converted to various nanostructures.[19−23] Recent theoretical and experimental studies[24−26] have shown that when ZnO is as thin as an atomic layer, its wurtzite structure can transform into a stable 2D monolayer structure similar to that of graphene, accordingly named graphene-like ZnO (or g-ZnO).[27−31] The structure of g-ZnO is chemically stable according to both theoretical calculations and experimentation. When synthesized as large-area nanosheets, the application range of g-ZnO is broadened owing to the expansion of its surface area.

In this study, we proposed the synthesis of $Zn(OH)_2$ nanosheets, with a thickness of several nanometers and micrometer size, via the proposed surfactant-assisted method to induce the growth of underlying nanostructures using a surfactant layer as a soft template at the water−air interface. Sodium hexadecyl sulfate (SHS) solution was used to synthesize $Zn(OH)_2$ nanosheets, with the synthesis of the nanosheets being driven by a floating anionic sulfate layer. When the synthesized $Zn(OH)_2$ nanosheet underwent additional annealing, its chemical state changed to form a ZnO-dominant sheet. In addition, control of the shape and thickness of the synthesized nanosheets was realized by varying the SHS concentration. Furthermore, oxygen evolution reaction (OER) using the morphologically controlled ZnO/$Zn(OH)_2$ nanosheets as catalysts was also studied.

RESULTS AND DISCUSSION

$Zn(OH)_2$ nanosheets were synthesized by the ionic layer epitaxy (ILE) method,[15−18] in which ionized molecules of SHS self-assemble at the water−air interface. Consequently, during the growth of $Zn(OH)_2$ nanosheets, ionized SHS molecules self-assembled into a highly packed monolayer at the surface of

Received: June 30, 2022
Accepted: September 19, 2022
Published: September 30, 2022

https://doi.org/10.1021/acsomega.2c04108
ACS Omega 2022, 7, 35834−35839

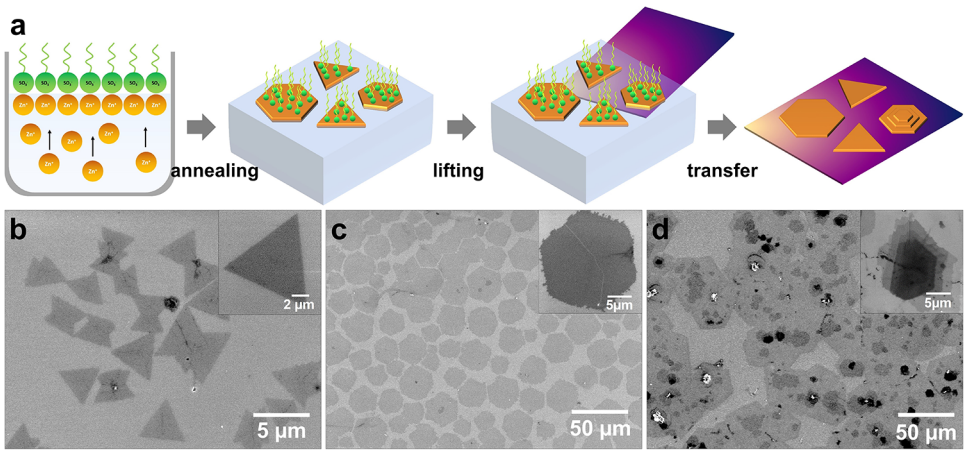

Figure 1. Synthesis of $Zn(OH)_2$ nanosheets. (a) Schematic illustration of nanosheet formation at the water−air interface. The synthesized nanosheets are transferred into an arbitrary substrate via scooping. SEM images of the (b) triangular, (c) hexagonal, and (d) p-hexagonal nanosheets.

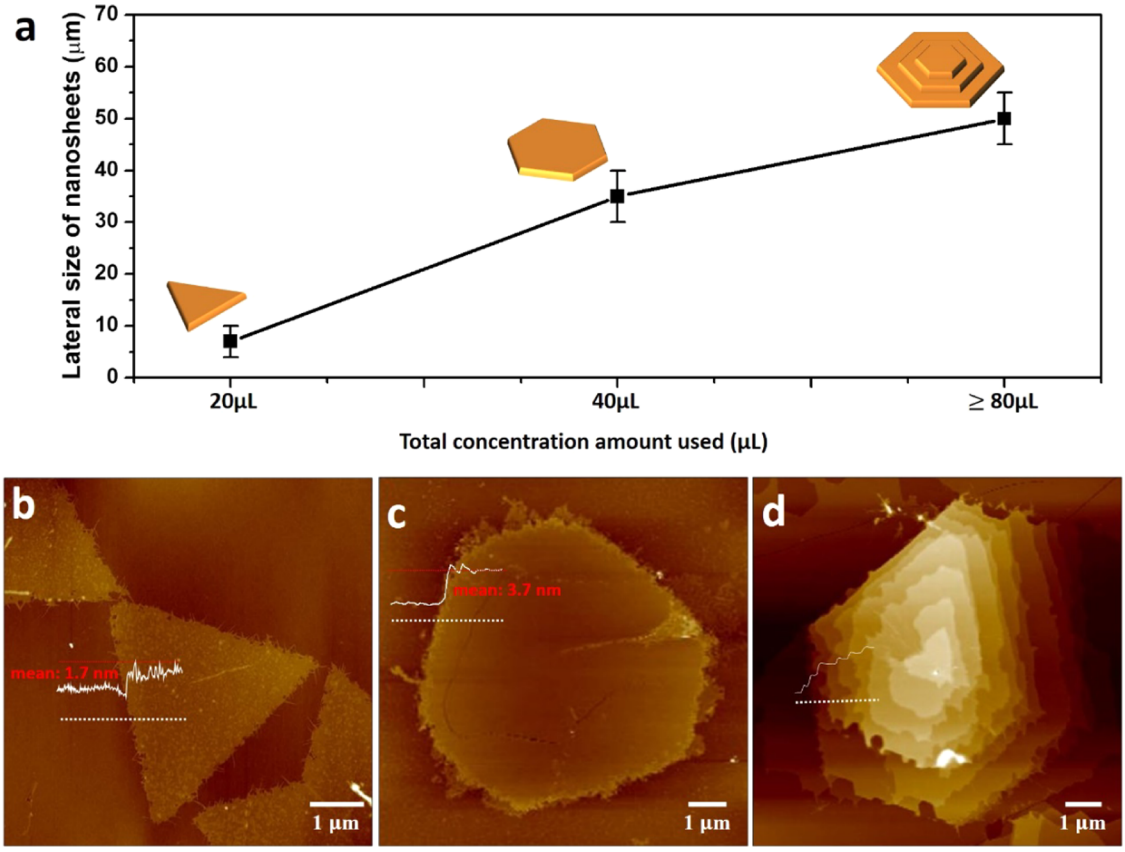

Figure 2. Size determination of $Zn(OH)_2$ nanosheets. (a) Average size of each nanosheet. (b−d) AFM topography images showing the nanometer thickness of the nanosheets with height profiles along each inset dashed lines.

water, forming a negatively charged ionic layer. As a result, positive Zn^+ ions were attracted to the interface, forming nanosheets. Figure 1a shows a schematic of the ILE method for $Zn(OH)_2$ nanosheets. In the growth process, the nanosheets were dipped and lifted out of the water−air interface using an arbitrary substrate to synthesize triangular, hexagonal, and pyramid-like hexagonal (p-hexagonal) nanosheets, depending on the concentration of SHS. Figure 1b,d show the scanning electron microscopy (SEM) images of the nanosheets transferred onto an SiO_2/Si substrate. The unilateral triangular and hexagonal structures contained p-hexagonal nanosheets with distinct morphologies. The insets in Figure 1b,d show magnified SEM images of their morphologies.

To study the effect of SHS concentration on the lateral size and thickness of the $Zn(OH)_2$ nanosheets, small areas on each substrate were randomly selected for morphological characterization. More than 100 nanosheets were analyzed for each sample; the results are shown in Figure 2. The shapes illustrated in Figure 2a show the simple morphology of each sheet. These shapes were dependent on the SHS concentration in chloroform during synthesis. When 20 μL of the surfactant was used for synthesis, triangular nanosheets were mainly

https://doi.org/10.1021/acsomega.2c04108
ACS Omega 2022, 7, 35834−35839

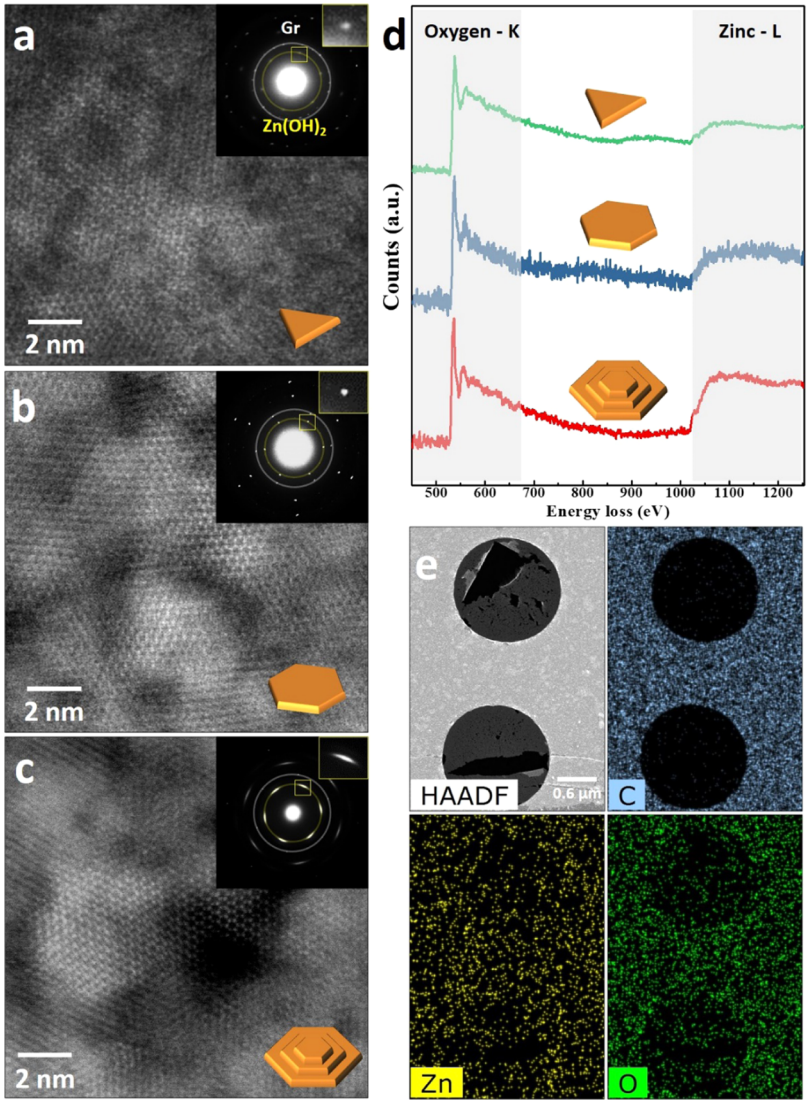

Figure 3. Structural characterization of $Zn(OH)_2$ nanosheets. (a–c) STEM-HAADF images with selected area electron diffraction (SAED) patterns of each sheet. (d) EEL spectrum of each nanosheet. (e) STEM-HAADF image with C, Zn, and O mappings. C mapping came from the supportive graphene sheet.

formed, and when more than 10 times the amount of SHS was used, hexagonal nanosheets were formed. The lateral size of the triangular nanosheets was small, averaging 10 ± 2 μm. The hexagonal nanosheets were comparatively larger and averaged 35 ± 5 μm. The p-hexagonal nanosheets were 50 ± 5 μm in size. Figure 2b–d show atomic force microscopy (AFM) images of the sample nanosheets with their thickness profiles. The thickness of the triangular nanosheets was up to approximately 1.7 nm, whereas the thickness of hexagonal nanosheets was up to 3.7 nm. The thickness of each layer of p-hexagonal nanosheets was similar to that of the hexagonal nanosheets.

A key factor in forming morphologies is the amount of the surfactant, such as SHS. These surfactant molecules are selective, which means they slow down the growth of certain material facets where surfactant molecules are adsorbed while promoting the growth of other facets. Thus, as shown in Figure S1a,b, triangular $Zn(OH)_2$ sheets were initially synthesized; however, as the amount of surfactant molecules increases, they get adsorbed to the corners of the crystallographic facets of the triangular sheets and thus guide their growth towards the hexagonal shape (Figure S1c,d). In addition, they can form a close-packed monolayer floating on water, where the Zn^+ ions are concentrated. This layer is an excellent template for the formation of $Zn(OH)_2$ nanosheets. As the Zn^+ ions react in this molecular layer and are influenced by increasing the number of surfactant molecules, the effective area available for the Zn^+ ions to react increases, and hence the lateral size of the synthesized nanosheets expands and thickens. Additionally, a high concentration of the precursor solution may also affect the shape, but it was not considered as a control condition in this study.

Figure 3 shows the characterization of the $Zn(OH)_2$ nanosheets using transmission electron microscopy (TEM). We used a monolayer graphene sheet as the substrate layer because the sheet did not fully cover the holes in the TEM grid. TEM images and selected area electron diffraction (SAED) patterns, acquired in a region of the field of view showing the nanosheet, are shown in Figure S2a,b. Further, Figure 3a,c show scanning transmission electron microscopy high-angle annular dark field (STEM-HAADF) images of each morphologically shaped nanosheet with SAED patterns. As a

https://doi.org/10.1021/acsomega.2c04108
ACS Omega 2022, 7, 35834–35839

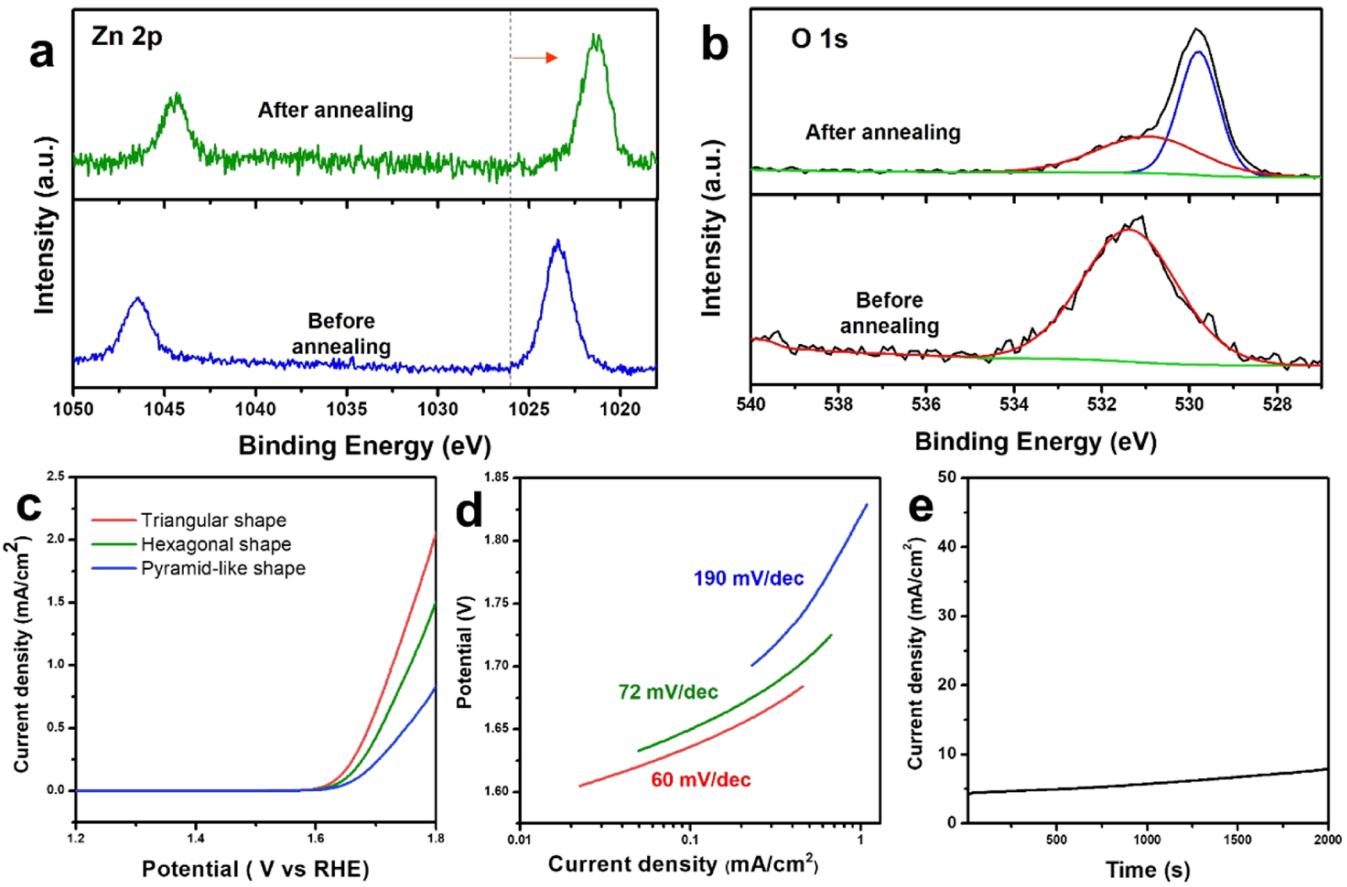

Figure 4. XPS spectrum of the as-synthesized $Zn(OH)_2$ nanosheets, annealed at 400 °C. (a) Zn 2p peaks and (b) O 1s peaks of the as-synthesized $Zn(OH)_2$ nanosheets before and after annealing at 400 °C. (c) Polarization curves of ZnO/$Zn(OH)_2$ nanosheets and (d) Tafel slopes plotted from polarization curve data. (e) Chronopotentiometric consequence (responding potential generating current density vs operation time) of triangular shapes.

graphene sheet was transferred onto the TEM grid before the transfer of the $Zn(OH)_2$ nanosheet, the SAED patterns simultaneously showed the graphene pattern (indicated by a white line) and the $Zn(OH)_2$ pattern (indicated by a yellow line). Comparing each image with the SAED patterns, the lattice of each sheet is the same (Figure S2c); in particular, only the SAED pattern of the p-hexagonal nanosheet is broadened (see insets marked by yellow boxes in Figure 3b,c). This indicates that the crystal orientation range of the p-hexagonal sheet was widened, whereas the triangular and hexagonal sheets had spots in the SAED pattern. These results suggest that an increase in the overall thickness of the synthesized sheet affects the periodicity of its orientation rather than the crystallinity. The electron energy loss (EEL) and energy dispersive X-ray spectroscopy (EDS) mapping analysis spectrum of each $Zn(OH)_2$ sheet indicated the absence of any other impurities (Figure 3d,e) on the graphene sheet and confirmed the presence of both Zn and O. The O−K edge peak located at approximately 532 eV corresponds to oxygen atoms bonded to Zn in the $Zn(OH)_2$ nanosheet (Figures 3d and S2d,e). The inset of Figure S2e shows the C−K edge with π^* and σ^* peaks in each sheet, confirming the presence of graphene behind the nanosheets.

In addition, X-ray photoelectron spectroscopy (XPS) was used to gain insight into the oxidation state of the nanosheets (Figure 4). The Zn $2p_{3/2}$ and $2p_{1/2}$ peaks of the as-synthesized $Zn(OH)_2$ nanosheet appear at 1023.4 and 1046.5 eV, which indicates that $Zn(OH)_2$ is dominant (Figure 4a). The O 1s peak at 531.4 eV indicates that the Zn atoms are bonded to the OH^- group (Figure 4b). After annealing the as-synthesized nanosheets under an air atmosphere at 400 °C for 4 h, the peak of Zn $2p_{3/2}$ shifted to 1021.3 eV, indicating the formation of ZnO (Figure 4a). The XPS O 1s spectra of the as-synthesized $Zn(OH)_2$ nanosheets obtained using ILE showed a symmetric peak, however, the peak became asymmetrical after annealing. The deconvolution of O 1s exhibits two clear peaks located at binding energies of 529.5 and 531.1 eV, which is attributed to oxygen in the wurtzite−ZnO crystal and oxygen vacancies, respectively (Figure 4b). The shift of Zn 2p towards lower binding energy is also attributed to the formation of oxygen vacancies. The XPS results were closely related to the oxygen evolution reaction (OER).

Polarization curves of the synthesized ZnO-dominant nanosheets with various shapes were obtained in 1 M KOH to investigate their catalytic activities in OER. As shown in Figure 4, the triangular ZnO-dominant nanosheets showed the most promising performance of the different morphologies, obtaining an overpotential of 1.6 V (vs reversible hydrogen electrode (RHE)) and a Tafel slope of 60 mV dec^{-1}. The OER mechanism can be explained in several ways as follows. Since oxygen vacancies serve as H_2O adsorption sites and transition metals can induce more active sites in metal hydroxides, combining the two factors improves the catalytic activity.[32] As the oxygen concentration decreases, the OER performance also

https://doi.org/10.1021/acsomega.2c04108
ACS Omega 2022, 7, 35834−35839

decreases (Figure S3). Although the performance is not exceptional, there are very few reports on the OER performance of two-dimensional ZnO-dominant nanosheets. Therefore, these results can be used to expand their application in the future.

CONCLUSIONS

This study demonstrates the results of controlling the morphology of $Zn(OH)_2$ nanosheets using varying amounts of surfactant molecules. Additionally, we suggested a method for controlling the thickness and shape of the synthesized $Zn(OH)_2$ nanosheets by controlling the density of hexadecyl sulfates. The crystal structures of the synthesized $Zn(OH)_2$ nanosheets for each morphology were consistent and were transformed into ZnO-dominant nanosheets by additional heat treatment. Furthermore, catalytic properties of the nanosheets in OER were studied, and in particular, triangular structure displayed the most optimal OER performance owing to the presence of additional oxygen vacancies and active sites. This technique shows great promise as a versatile synthetic route for fabricating morphologically controlled nanosheets from various inorganic materials including van der Waals solids.

MATERIALS AND METHODS

Preparation of $Zn(OH)_2$ Nanosheets. To synthesize $Zn(OH)_2$ nanosheets, 5 g chloroform solution with 0.002 g sodium hexadecyl sulfate (SHS) was added to the surface of the aqueous solution containing $Zn(NO_3)_2$ and hexamethylenetetramine (HMTA) as precursors for $Zn(OH)_2$. This precursor solution was prepared by mixing 35 mL of deionized water containing 0.0332 g of zinc nitrate and 35 mL of deionized water containing 0.0248 g of HMTA. This solution is contained in a Glasslock (size: 74 × 74 × 63.5 mmH) and placed in a convection oven at 70 °C for typically 180 min. An arbitrary substrate, typically a SiO_2-coated Si wafer, was then used to scoop the nanosheets from the water−air interface for subsequent characterization. If only the amount of SHS added chloroform solution is added under control as shown in Figure 2, morphologically controlled nanosheets can be obtained.

Characterization Using SEM, AFM, and XPS. The morphology and chemical properties of $Zn(OH)_2$ nanosheets were characterized by scanning electron microscope (SEM, FEI Quanta 3D FIB with acceleration voltage of 5 kVm beam current of 0.11 nA), atomic force microscope (AFM, Veeco Multimode V), and X-ray photoemission spectroscopy (XPS, Thermofisher K-alpha). XPS data were obtained from the nanosheets transferred onto 50 nm-thick platinum coated-Si substrate to minimize the signal from the native oxide of Si substrates. Peak deconvolution was carried out after background subtraction using Shirley background.

TEM Observations and STEM−EELS spectra. Specimens were analyzed using a TF30ST, which was operated at an 300 kV and an aberration-corrected FEI Titan Cubed TEM (FEI Titan3 G2 60-300), which was operated at an 80 kV acceleration voltage with a monochromator. The microscope provided a sub-Angstrom resolution at 80 kV and −13 ± 0.5 μm of spherical aberration (Cs). Typical electron beam densities were adjusted to ∼6 × 105 e^- nm^{-2}. The atomic images were taken using a white atom contrast to obtain the actual atom positions under the properly focused conditions needed for direct image interpretation. STEM-HAADF images and EELS spectra were recorded with a monochromatic beam at 80 kV with a probe size of 1.5 nm and an energy resolution of 0.8 eV, as measured from the full-width-at-half-maximum of the zero-loss peak.

Electrochemical Measurements. The catalytic performance of the $ZnO/Zn(OH)_2$ nanosheets for oxygen evolution reaction was performed by using a three-electrode system connected to a potentiostat (Zive SP1). The counter electrode was platinum wire and the reference electrode was Hg/HgO electrode. Linear sweep voltammetry (LSV) measurements were gained in an alkali solution (1 M KOH) at room temperature at a scan rate of 5 mV s^{-1}. For the purpose of comparison, the catalytic performance of materials was tested on a fluorine-doped tin oxide (FTO) working electrode under similar conditions. All potential measurements were converted to the reversible hydrogen electrode (RHE) based on the following formula $E_{RHE} = E_{Hg/HgO} - 0.11 + 0.059$ pH (in volts). It should be noted that all of the current densities were normalized on the electrode areas. *The preparation of electrodes.* Conducting fluorine-doped tin oxide (FTO) substrates are used to support catalysts. The FTO substrates are washed by bath sonication in water and IPA for 10 min each. The as-synthesized ZnO nanosheets in DI water are delaminated onto FTO substrates and dried in ambient at 500 °C for 2 h.

ASSOCIATED CONTENT

Supporting Information

The Supporting Information is available free of charge at https://pubs.acs.org/doi/10.1021/acsomega.2c04108.

Additional experimental figures showing the formation mechanism, crystal structures, and XPS O 1s spectra (PDF)

AUTHOR INFORMATION

Corresponding Authors

A-Rang Jang − *Division of Electrical, Electronic and Control Engineering, Kongju National University, Cheonan 31080, Republic of Korea;* orcid.org/0000-0002-0758-9757; Email: arjang@kongju.ac.kr

Gyeong Hee Ryu − *School of Materials Science and Engineering, Gyeongsang National University, Jinju 52828, Republic of Korea;* orcid.org/0000-0002-8992-8694; Email: gh.ryu@gnu.ac.kr

Authors

Gyu Hyun Jeong − *School of Materials Science and Engineering, Gyeongsang National University, Jinju 52828, Republic of Korea*

Hye Soung Jang − *School of Materials Science and Engineering, Gyeongsang National University, Jinju 52828, Republic of Korea*

Jong Chan Yoon − *Department of Materials Science and Engineering, Ulsan National Institute of Science and Technology (UNIST), Ulsan 44919, Republic of Korea; Center for Multidimensional Carbon Materials, Institute for Basic Science (IBS), Ulsan 44919, Republic of Korea;* orcid.org/0000-0003-1871-600X

Zonghoon Lee − *Department of Materials Science and Engineering, Ulsan National Institute of Science and Technology (UNIST), Ulsan 44919, Republic of Korea; Center for Multidimensional Carbon Materials, Institute for Basic Science (IBS), Ulsan 44919, Republic of Korea;* orcid.org/0000-0003-3246-4072

https://doi.org/10.1021/acsomega.2c04108
ACS Omega 2022, 7, 35834−35839

Jieun Yang − *Department of Chemistry and Research Institute of Basic Sciences, Kyung Hee University, Seoul 02447, Republic of Korea*

Complete contact information is available at: https://pubs.acs.org/10.1021/acsomega.2c04108

Notes

The authors declare no competing financial interest.

■ ACKNOWLEDGMENTS

This work was supported by the National Research Foundation of Korea (NRF) grant funded by the Korea government (MSIT) (Nos. 2020R1G1A1099542 and 2022R1F1A1068161) and "Regional Innovation Strategy (RIS)" through the National Research Foundation of Korea (NRF) funded by the Ministry of Education (MOE) (2021RIS-003). We would like to thank Editage (www.editage.co.kr) for English language editing.

■ REFERENCES

(1) Zhang, H. Ultrathin Two-Dimensional Nanomaterials. *ACS Nano* **2015**, *9*, 9451−9469.
(2) Zhang, X.; Xie, X.; Wang, H.; Zhang, J.; Pan, B.; Xie, Y. Enhanced Photoresponsive Ultrathin Graphitic-Phase C_3N_4 Nanosheets for Bioimaging. *J. Am. Chem. Soc.* **2013**, *135*, 18−21.
(3) Ramakrishna Matte, H. S. S.; Gomathi, A.; Manna, A. K.; Late, D. J.; Datta, R.; Pati, S. K.; Rao, C. N. R. MoS_2 and WS_2 Analogues of Graphene. *Angew. Chem., Int. Ed.* **2010**, *49*, 4059−4062.
(4) Rao, C. N. R.; Sood, A. K.; Subrahmanyam, K. S.; Govindaraj, A. Graphene: The New Two-Dimensional Nanomaterial. *Angew. Chem., Int. Ed.* **2009**, *48*, 7752−7777.
(5) Lei, W.; Portehault, D.; Liu, D.; Qin, S.; Chen, Y. Porous Boron Nitride Nanosheets for Effective Water Cleaning. *Nat. Commun.* **2013**, *4*, No. 1777.
(6) Lukowski, M. A.; Daniel, A. S.; Meng, F.; Forticaux, A.; Li, L.; Jin, S. Enhanced Hydrogen Evolution Catalysis from Chemically Exfoliated Metallic MoS_2 Nanosheets. *J. Am. Chem. Soc.* **2013**, *135*, 10274−10277.
(7) Radisavljevic, B.; Radenovic, A.; Brivio, J.; Giacometti, V.; Kis, A. Single-Layer MoS_2 Transistors. *Nat. Nanotechnol.* **2011**, *6*, 147−150.
(8) Fang, H.; Bechtel, H. A.; Plis, E.; Martin, M. C.; Krishna, S.; Yablonovitch, E.; Javey, A. Quantum of Optical Absorption in Two-Dimensional Semiconductors. *Proc. Natl. Acad. Sci. U.S.A.* **2013**, *110*, 11688−11691.
(9) Zhang, Y.; Zhang, L.; Zhou, C. Review of Chemical Vapor Deposition of Graphene and Related Applications. *Acc. Chem. Res.* **2013**, *46*, 2329−2339.
(10) Lee, K. H.; Shin, H.-Y.; Lee, J.; Lee, I.-Y.; Kim, G.-H.; Choi, J.-Y.; Kim, S.-W. Large-Scale Synthesis of High-Quality Hexagonal Boron Nitride Nanosheets for Large-Area Graphene Electronics. *Nano Lett.* **2012**, *12*, 714−718.
(11) Lee, Y.-H.; Zhang, X.-Q.; Zhang, W.; Chang, M.-T.; Lin, C.-T.; Chang, K.-D.; Yu, Y.-C.; Wang, J. T.-W.; Chang, C.-S.; Li, L.-J.; Lin, T.-W. Synthesis of Large-Area MoS_2 Atomic Layers with Chemical Vapor Deposition. *Adv. Mater.* **2012**, *24*, 2320−2325.
(12) Wang, F.; Wang, X. Mechanisms in the Solution Growth of Free-Standing Two-dimensional Inorganic Nanomaterials. *Nanoscale* **2014**, *6*, 6398−6414.
(13) Dutour Sikirić, M.; Füredi-Milhofer, H. The Influence of Surface Active Molecules on the Crystallization of Biominerals in Solution. *Adv. Colloid Interface Sci.* **2006**, *128*−*130*, 135−158.
(14) Yin, Y.; Alivisatos, A. P. Colloidal Nanocrystal Synthesis and the Organic-Inorganic Interface. *Nature* **2005**, *437*, 664−670.
(15) Wang, F.; Seo, J.-H.; Luo, G.; Starr, M. B.; Li, Z.; Geng, D.; Yin, X.; Wang, S.; Fraser, D. G.; Morgan, D.; Ma, Z.; Wang, X. Nanometre-Thick Single-Crystalline Nanosheets Grown at the Water-Air Interface. *Nat. Commun.* **2016**, *7*, No. 10444.
(16) Wang, Y.; Shi, Y.; Zhang, Z.; Carlos, C.; Zhang, C.; Bhawnani, K.; Li, J.; Wang, J.; Voyles, P. M.; Szlufarska, I.; Wang, X. Bioinspired Synthesis of Quasi-Two-Dimensional Monocrystalline Oxides. *Chem. Mater.* **2019**, *31*, 9040−9048.
(17) Wang, F.; Seo, J.-H.; Ma, Z.; Wang, X. Substrate-Free Self-Assembly Approach Toward Large-Area Nanomembranes. *ACS Nano* **2012**, *6*, 2602−2609.
(18) Wang, F.; Jakes, J. E.; Geng, D.; Wang, X. Spontaneous Phase Transformation and Exfoliation of Rectangular Single-Crystal Zinc Hydroxy Dodecylsulfate Nanomembranes. *ACS Nano* **2013**, *7*, 6007−6016.
(19) Djurišić, A.; Leung, Y. H. Optical Properties of ZnO Nanostructures. *Small* **2006**, *2*, 944−961.
(20) Schmidt-Mende, L.; MacManus-Driscoll, J. L. ZnO-Nanostructures, Defects, and Devices. *Mater. Today* **2007**, *10*, 40−48.
(21) Djurišić, A. B.; Chen, X.; Leunga, Y. H.; Ching Ng, A. N. ZnO Nanostructures: Growth, Properties and Applications. *J. Mater. Chem.* **2012**, *22*, 6526−6535.
(22) Xu, S.; Wang, Z. L. One-Dimensional ZnO Nanostructures: Solution Growth and Functional Properties. *Nano Res.* **2011**, *4*, 1013−1098.
(23) Xu, L.; Guo, Y.; Liao, Q.; Zhang, J.; Xu, D. Morphological Control of ZnO Nanostructures by Electrodeposition. *J. Phys. Chem. B* **2005**, *109*, 13519−13522.
(24) Claeyssens, F.; Freeman, C. L.; Allan, N. L.; Sun, Y.; Ashfolda, M. N. R.; Harding, J. H. Growth of ZnO Thin Films-Experiment and Theory. *J. Mater. Chem.* **2005**, *15*, 139−148.
(25) Tusche, C.; Meyerheim, H. L.; Kirschner, J. Observation of Depolarized ZnO(0001) Monolayers: Formation of Unreconstructed Planar Sheets. *Phys. Rev. Lett.* **2007**, *99*, No. 026102.
(26) Tu, Z. C.; Hu, X. Elasticity and Piezoelectricity of Zinc Oxide Crystals, Single Layers, and Possible Single-Walled Nanotubes. *Phys. Rev. B* **2006**, *74*, No. 035434.
(27) Yoon, J. C.; Lee, Z.; Ryu, G. H. Atomic Arrangements of Graphene-like ZnO. *Nanomaterials* **2021**, *11*, No. 1833.
(28) Ta, H. Q.; Zhao, L.; Pohi, D.; Pang, J.; Trzebicka, B.; Rellinghaus, B.; Pribat, D.; Gemming, T.; Liu, Z.; Bachmatiuk, A.; Rümmeli, N. H. Graphene-Like ZnO: A Mini Review. *Crystals* **2016**, *6*, No. 100.
(29) Hong, H.-K.; Jo, J.; Hwang, D.; Lee, J.; Kim, N. Y.; Son, S.; Kim, J. H.; Jin, M.-J.; Jun, Y. C.; Erni, R.; Kwak, S. K.; Yoo, J.-W.; Lee, Z. Atomic Scale Study on Growth and Heteroepitaxy of ZnO Monolayer on Graphene. *Nano Lett.* **2017**, *17*, 120−127.
(30) Son, S.; Cho, Y.; Hong, H.-K.; Lee, J.; Kim, J. H.; Kim, K.; Lee, Y.; Yoon, A.; Shin, H.-J.; Lee, Z. Spontaneous Formation of a ZnO Monolayer by the Redox Reaction of Zn on Graphene Oxide. *ACS Appl. Mater. Interfaces* **2020**, *12*, 54222−54229.
(31) Quang, H. T.; Bachmatiuk, A.; Dianat, A.; Ortmann, F.; Zhao, J.; Warner, J. H.; Eckert, J.; Cunniberti, G.; Rümmeli, N. H. In Situ Observations of Free-Standing Graphene-like Mono- and Bilayer ZnO Membranes. *ACS Nano* **2015**, *9*, 11408−11413.
(32) Xu, L.; Jiang, Q.; Xiao, Z.; Li, Z.; Huo, J.; Wang, S.; Dai, L. Plasma-Engraved Co_3O_4 Nanosheets with Oxygen Vacancies and High Surface Area for the Oxygen Evolution Reaction. *Angew. Chem.* **2016**, *128*, 5363−5367.